International Journal of Thermal Sciences 208 (2025) 109443

Contents lists available at ScienceDirect

International Journal of Thermal Sciences

journal homepage: www.elsevier.com/locate/ijts

Thermal characterisation of isotopic heat sources for enhanced thermophotovoltaic systems

Zhiheng Xu [a,b,*], Jiyu Wang [a], Yuqiao Wang [c], Shifan Zhu [c], Hongyu Wang [a], Dandan Yang [d], Yunpeng Liu [a], Xiaobin Tang [a,b,**]

[a] Department of Nuclear Science and Technology, Nanjing University of Aeronautics and Astronautics, Nanjing, 211106, China
[b] Key Laboratory of Nuclear Technology Application and Radiation Protection in Aerospace, Ministry of Industry and Information Technology, Nanjing, 211106, China
[c] Research Center for Nano Photoelectrochemistry and Devices, School of Chemistry and Chemical Engineering, Southeast University, Nanjing, 211189, China
[d] Institute of Innovation Materials and Energy, School of Chemistry and Chemical Engineering, Yangzhou University, Yangzhou, 225002, China

ARTICLE INFO

Keywords:
Thermophotovoltaic system
Heat source
Selective coating
Temperature distribution

ABSTRACT

Radioisotope thermophotovoltaics (RTPVs) are playing an increasingly important role in the energy supply for deep space exploration. The output performance of RTPVs can be significantly improved by increasing the surface temperature of isotopic heat sources and reducing the high-temperature degradation effect of the thermophotovoltaic cells. This work proposes methods such as selective emission coating and adjusting heat source structure to improve heat source temperature and optimize heat distribution. Results showed that the surface temperature of the heat source could generally reach more than 1000 K by using the selective coating when the thermal power of the isotopic heat source was 500 W. The use of selective coatings can also make the thermophotovoltaic cells closer to the heat source, and the volume of RTPVs could be reduced from 1.23×10^{-3} m^3 to 0.49×10^{-3} m^3, with a reduction of ~60 %. Under the condition of W@SiO_2 selective coating and 500 W heat source, RTPVs could produce the maximum output power of 22 mW/cm^2 when the distance between the InGaAs cell and the heat source is 2 cm. The results provided effective guidance for the design of the heat source and miniaturization of RTPVs in space applications.

1. Introduction

Space exploration has recently ushered in a new round of upsurge in recent years. To meet the needs of various tasks, long-term self-sufficient power supply is urgently needed [1,2]. With the development of nuclear power technology, radioisotope thermophotovoltaics (RTPVs) have been considered as the favorable energy supply method, due to its high energy conversion efficiency and long lifetime [3–6]. RTPVs mainly convert infrared light generated by isotopic heat sources into electrical energy through semiconductor photovoltaic (PV) cells [7]. As a static energy conversion method, RTPV has higher conversion efficiency than the conventional thermoelectric methods [8–10], indicating its excellent advantages as the next generation space power source.

RTPV consists of isotopic heat source, thermo-optical conversion coating, and PV cell [11]. As the energy source of RTPV, $^{238}PuO_2$ was widely used as the fuel material due to its high specific power and long half-life [8]. Given the limited thermal power of isotopic heat source, the electrical output of RTPV can be effectively improved by optimizing measures to generate higher heat source temperature. Schock et al. studied the performance of RTPV with the general purpose heat source (GPHS) power of 62.5–250 W and made detailed numerical values for space missions [8,12]. Morgan et al. used more GPHSs to obtain greater output power [13]. Cheon et al. studied the influence of different cladding materials and structures on the temperature of the heat source [14]. In addition, numerous studies also have been conducted on the coating design. Wang et al. designed a Ta3%W photonic crystal outside the heat source and studied the variation in the temperature of the heat source and output power [15,16]. Lee et al. discussed the performance impact of two-dimensional tantalum emitter and tandem filter [17]. In our previous work, systematic studies have been conducted around silicon coating [18], spinel-type ferrite coating [19], and W@SiO_2 coating [20] for RTPV performance improvement. In general, improving the emissivity and thermal power of radioisotope heat sources and optimizing their structural design are effective ways to increase their surface temperature. However, detailed comparative analysis and research on

* Corresponding author. Department of Nuclear Science and Technology, Nanjing University of Aeronautics and Astronautics, Nanjing 211106, China.
** Corresponding author. Department of Nuclear Science and Technology, Nanjing University of Aeronautics and Astronautics, Nanjing 211106, China.
E-mail addresses: xuzhiheng@nuaa.edu.cn (Z. Xu), tangxiaobin@nuaa.edu.cn (X. Tang).

https://doi.org/10.1016/j.ijthermalsci.2024.109443
Received 15 June 2024; Received in revised form 31 August 2024; Accepted 23 September 2024
Available online 25 September 2024

Nomenclature

Symbols

T	Temperature, K
ρ	Density, kg/cm^3
C_p	Specific heat at constant pressure, J/(kg·K)
u	Velocity, m/s
q	Heat flux, W/m^2
Q	Heat, W
G	Irradiance, W/m^2
κ	Thermal conductivity, W/(m·K)
ε	Surface emissivity of heat source
I	Power density of radiation, W/(m^2·nm)
k	Boltzmann constant, J/K
h	Planck's constant, J·s
λ	Wavelength, nm
c	Speed of light, m/s
J	Output current density, A/cm^2
J_0	Reverse saturation current density, A/cm^2
J_{sc}	Short-circuit current density, A/cm^2
V	Output voltage, V
V_{oc}	Open-circuit voltage, V
P	Power density, W/cm^2
E_g	Bandgap, eV
T_c	Temperature of TPV cell, K
T_{max}	Maximum surface temperature of heat source, K
P_{max}	Maximum output power density, W/cm^2

Abbreviations

RTPV	Radioisotope thermophotovoltaic
GPHS	General Purpose Heat Source
PF	Packing Factor
QE	Quantum Efficiency

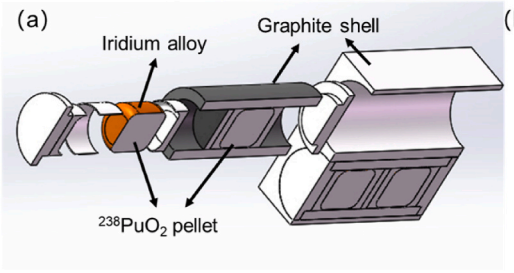

(b)

Radioisotope	Pu-238
Chemical compound	$^{238}PuO_2$
Melting point	2353 K
Half-life	87.7 a
Power per activity	32000 μW/Ci
Specific activity	15 Ci/g
Mass density	11.5 g/cm^3

Fig. 1. (a) Basic structure and (b) material properties of the radioisotope heat source.

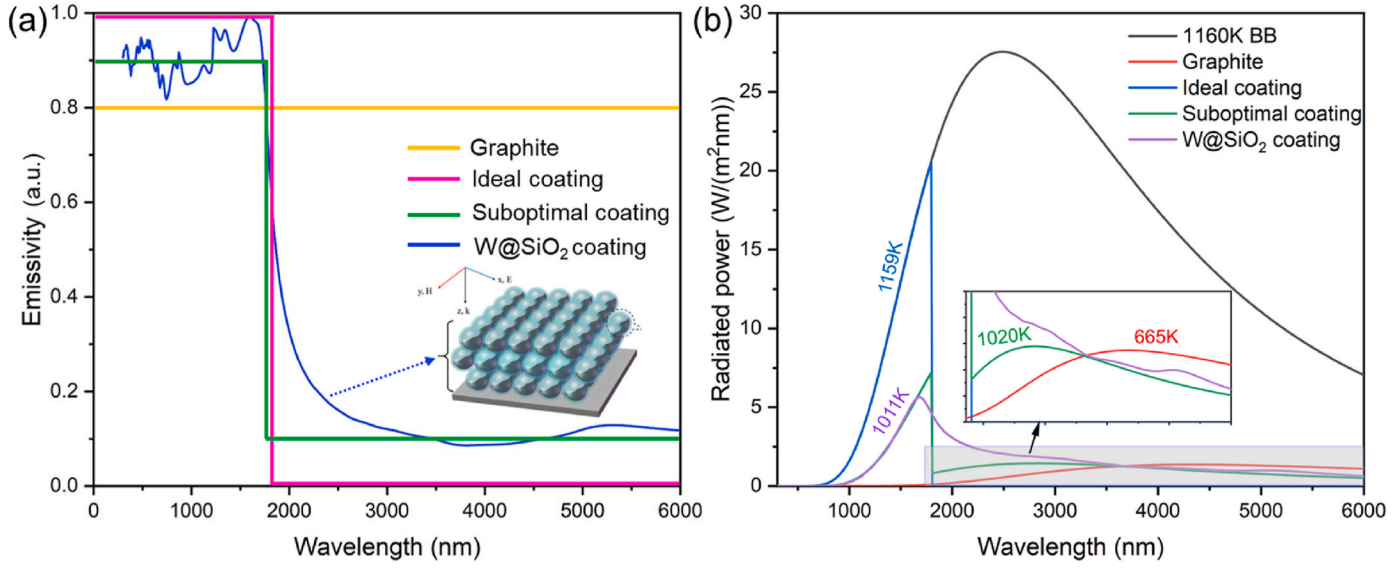

Fig. 2. (a) Emissivity spectra and (b) thermal radiation power spectra of the heat source with different coatings.

temperature rise of radioisotope heat source using such methods are still lacking. And the potential electrical output changes of RTPV caused by the rise in the temperature of the heat source are also unclear. Therefore, optimizing the research on temperature regulation of radioisotope heat source is greatly beneficial for RTPV application.

RTPV miniaturization is also an important future developmental trend to adapt to more space missions. Among such developments is the placement of the TPV cell closer to the heat source, which can make the internal transduction structure more compact. However, such process may also increase the negative impact of the high temperature of the heat source on the TPV cells, and the output power also decreases with the cell temperature [21]. Zhang et al. tested and compared the electrical characteristics of Ge, GaSb, and InGaAsSb cells in the temperature range of 303–307 K [22]. Peng et al. conducted a simulation study on the

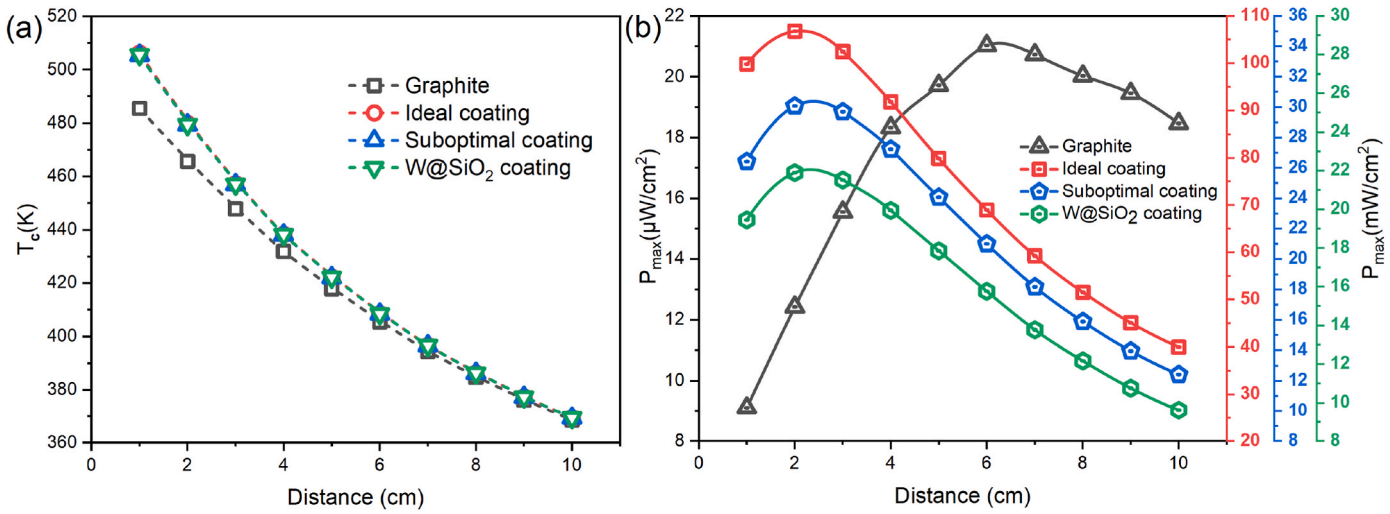

Fig. 3. Variation in (a) T_c and (b) P_{max} of InGaAs cell with the distance change under different coating emissivity.

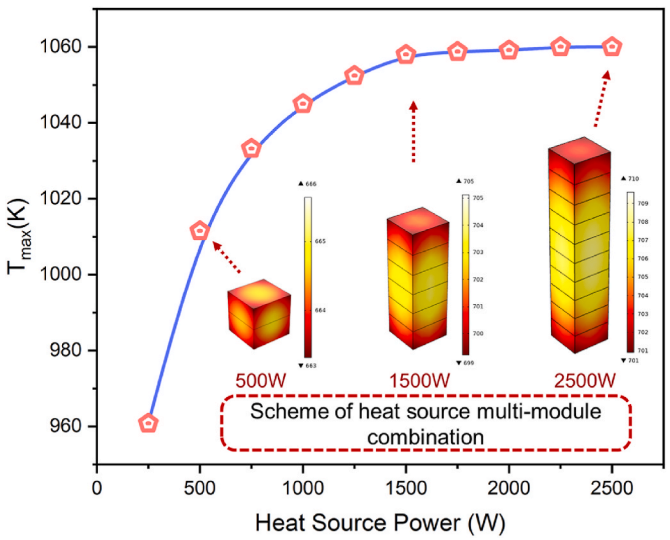

Fig. 4. Maximum surface temperature at various heat source power. Illustrations are temperature distribution diagrams of multi-module combination of heat source.

electrical properties of InGaAsSb cells at 200–400 K [23]. Etienne et al. analyzed the performance of GaSb cells in a higher temperature range (~600 K) and expected to reduce the temperature of GaSb cells by lowering the heat source temperature [24]. However, these studies focus on the TPV cell itself, but it cannot be denied that the thermal performance of the heat source plays a decisive role in the system structure design and electrical output performance. Studying the impact of distance between TPV cells and isotope heat sources can help closely integrate parameters such as heat source temperature, battery temperature, and the degree of miniaturization of RTPV. For RTPVs, the temperature of isotopic heat sources is usually expected to be above 1000 K [4]. When the temperature of TPV cells rises from 300 K to 500 K, the electrical output power density will decrease by nearly 80 % [24]. Therefore, increasing the temperature of the heat source, controlling the temperature of the TPV cell, and considering the miniaturization of the RTPV are very important to improve the electrical output performance of the RTPV.

In this work, the thermal distribution of heat source and its influence on the performance of RTPVs were analyzed by finite element method. The surface temperature of the heat source was optimized by adjusting the thermo-optical conversion coating, thermal power, and geometrical structure, thereby promoting the miniaturization of RTPVs and increasing the power density. The temperature and distance effects of the heat source on the TPV cell were analyzed in detail, and the electrical output of RTPV was further investigated.

2. Detailed simulations and experimental conditions

Fig. 1 shows the geometric structure and the material physical properties of the $^{238}PuO_2$ radioisotope heat source. The innermost layer was four $^{238}PuO_2$ pellets, each with a radius of 13.75 mm and a height of 27.5 mm. The outer layer of the $^{238}PuO_2$ pellet was wrapped with iridium alloy, and its thickness was 0.5 mm. The outermost layers were made of graphite, with a length of 97.2 mm, a width of 93.44 mm, and a height of 53.1 mm. Adding an appropriate coating on the surface of the radioisotope heat source can improve the thermo-optic performance, and the thickness of the coating is generally from nano to micro levels. A size of 1 × 1 cm^2 InGaAs-based TPV cells with TiO_2/SiO_2 antireflective film were selected as photoelectric conversion devices and designed to be 1 mm thick and placed parallel to the surface of the radioisotope heat source (Figs. S1–S3).

In the steady-state, solid heat transfer model and radiative heat transfer model were used for coupled analysis, and the material parameters available in the built-in material library and other reports were used for COMSOL simulation [25–27]. After setting the initial thermal power, the temperature distribution of the radioisotope heat source can be established as follows [28]:

$$\rho C_p u \cdot \nabla T + \nabla q = Q \tag{1}$$

$$q = -\kappa \nabla T \tag{2}$$

$$J = \varepsilon e_b(T) + \rho_d G \tag{3}$$

where ρ is the density, C_p is the specific heat at constant pressure, u is the velocity, T is the temperature, q is the heat flux, Q is the heat, κ is the thermal conductivity, J is the radiosity, ε is the emissivity, and G is the irradiance.

For RTPV, the emissivity of the heat source coatings is not constant but a wavelength-dependent function $\varepsilon(\lambda)$ that can be accurately simulated in COMSOL using multiple spectral bands. Thus, the emission spectrum becomes [29]:

$$I_{em}(\lambda, T) = \varepsilon(\lambda) \cdot I_{BB}(\lambda, T) = \frac{2\pi hc^2 \cdot \varepsilon(\lambda)}{\lambda^5} \times \frac{1}{e^{\frac{hc}{\lambda kT}} - 1} \tag{4}$$

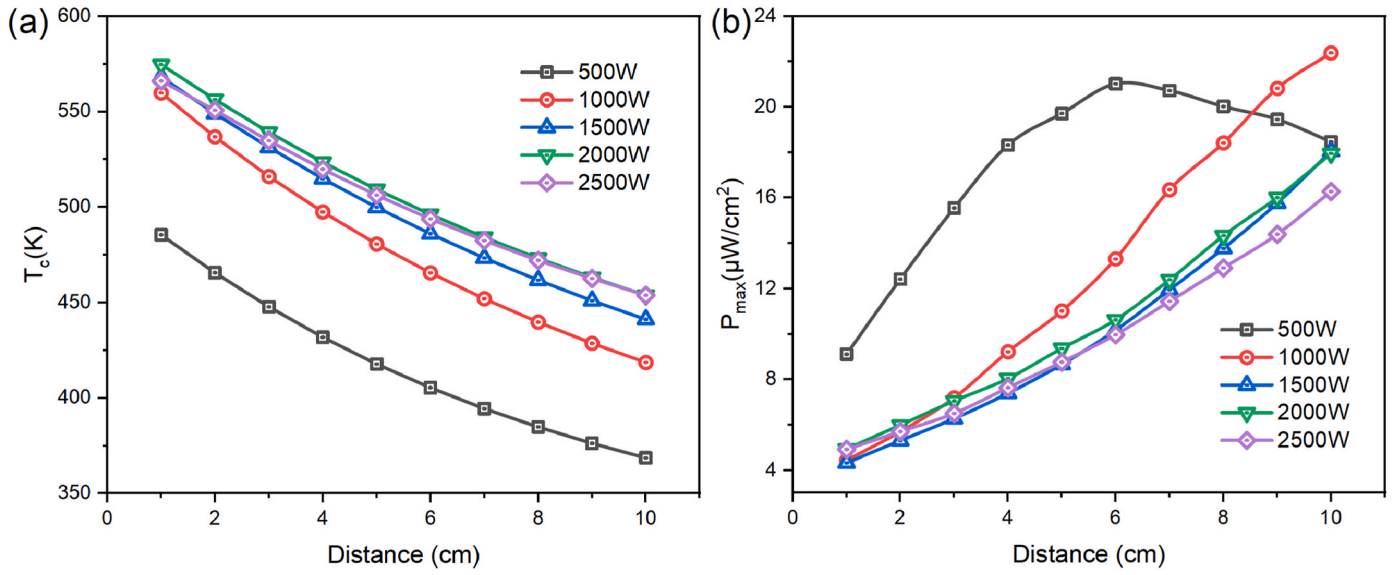

Fig. 5. Variation in (a) T_c and (b) P_{max} of InGaAs cell with the distance change under different thermal power of the heat sources.

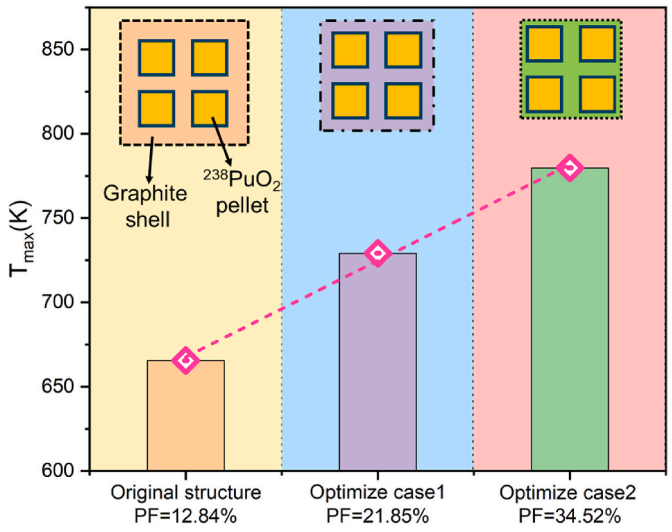

Fig. 6. T_{max} at various heat source structure. Illustrations are cross-sectional schematic diagrams of different heat source structures.

$$\varepsilon e_b(\lambda, T) = \int I_{em}(\lambda, T) d\lambda \tag{5}$$

where $I_{BB}(\lambda,T)$ is the blackbody radiation at temperature T obtained from Planck's law, h is Planck's constant, c is the speed of light, λ is the wavelength, and k is Boltzmann's constant.

The domain heat source was used to set the thermal power of $^{238}PuO_2$ pellets, and each pellet provided a thermal power of 62.5 W. The convection coefficient on the back of the TPV cell was set to 5 W/(m^2·K), and the ambient temperature was set to 293 K. In addition, the parallel sparse direct solver and fully coupled direct linear solver were used for the numerical study.

After the surface temperature of the radioisotope heat source and the irradiance received by the TPV cells were determined, the *J-V* and *P-V* curves of RTPV can be calculated according to the Shockley diode equation as follows:

$$J(V) = J_{sc} - J_0 \left[exp\left(\frac{qV}{kT_c}\right) - 1 \right] \tag{6}$$

$$P = J \times V \tag{7}$$

where J is the current density, J_{sc} is the short-circuit current density, J_0 represents the reverse saturation current density, q is the charge amount, V is the output voltage, T_c is the cell temperature, and P is the power density. J_0 is related to the bandgap (E_g) and T_c of the InGaAs cell. J_{sc} and J_0 can be calculated by the following formulas:

$$J_{sc} = q \int_0^{\infty} \frac{q\lambda}{hc} QE(\lambda) I_{em}(\lambda, T) d\lambda \tag{8}$$

$$J_0 = q \int_{E_g}^{\infty} \frac{2\pi E^2}{h^3 c^2 \left[exp\left(\frac{E}{kT_c}\right) - 1 \right]} dE \tag{9}$$

where $QE(\lambda)$ is the quantum efficiency of the TPV cell. When the TPV cell is at a certain distance from the heat source, the J_{sc} becomes:

$$J'_{sc} = \frac{G}{\varepsilon e_b(\lambda, T)} J_{sc} \tag{10}$$

Temperature mainly affects the bandgap of $In_{1-x}Ga_xAs$ cells, and E_g was determined as follows [30]:

$$E_g(x, T_c) = 0.42 + 0.625x - \left(\frac{5.8}{T_c + 300} - \frac{4.19}{T_c + 271}\right) \times 10^{-4} x T_c^2 - \left(\frac{4.19 \times 10^{-4} T_c^2}{T_c + 271}\right) + 0.475x^2 \tag{11}$$

where x is the concentration of Ga.

3. Results and discussion

3.1. Selective emission of heat source coatings

The thermal power of the radioisotope heat source was set to 500 W, and a thermo-optical conversion coating was added to emit infrared light. Gray body coating has consistent high emissivity in the whole wavelength range, while selective coating only shows high emissivity in the response band of the TPV cell. In order to study the degree and upper limit of the gain with different coatings on heat source temperature and RTPV output, as shown in Fig. 2(a), the emissivity of coating was set with four different models, namely, graphite coating, ideal coating, suboptimal coating, and W@SiO_2 coating. Graphite itself as the heat

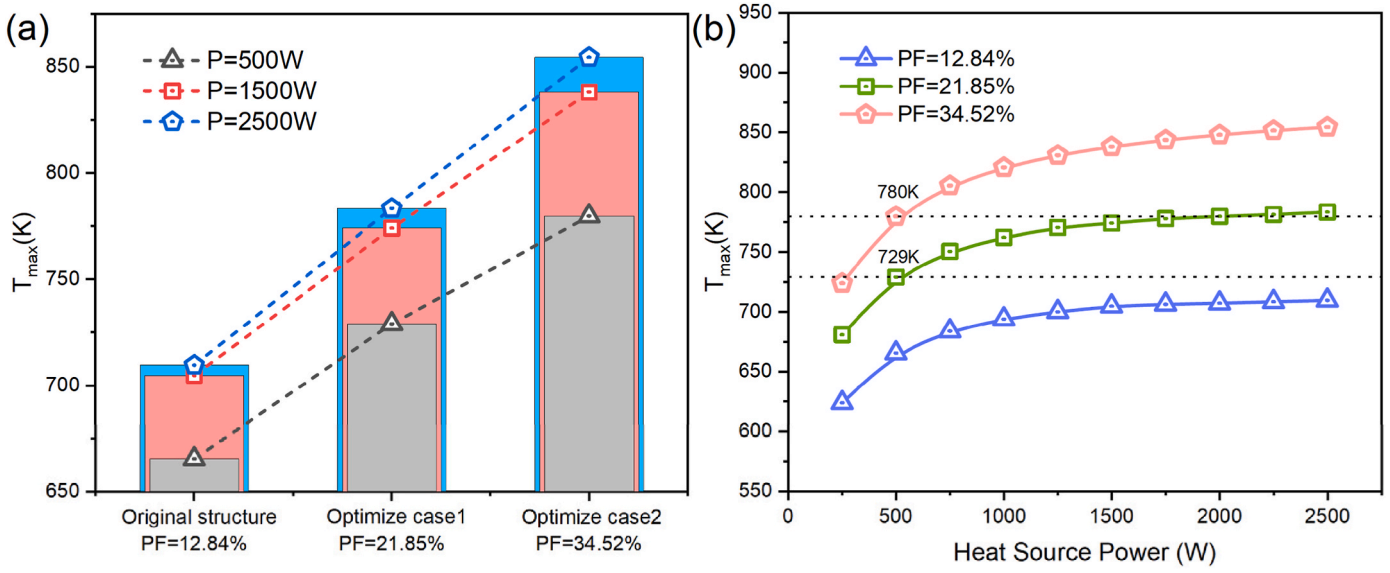

Fig. 7. Influence of thermal power on T_{max} under different heat source structures.

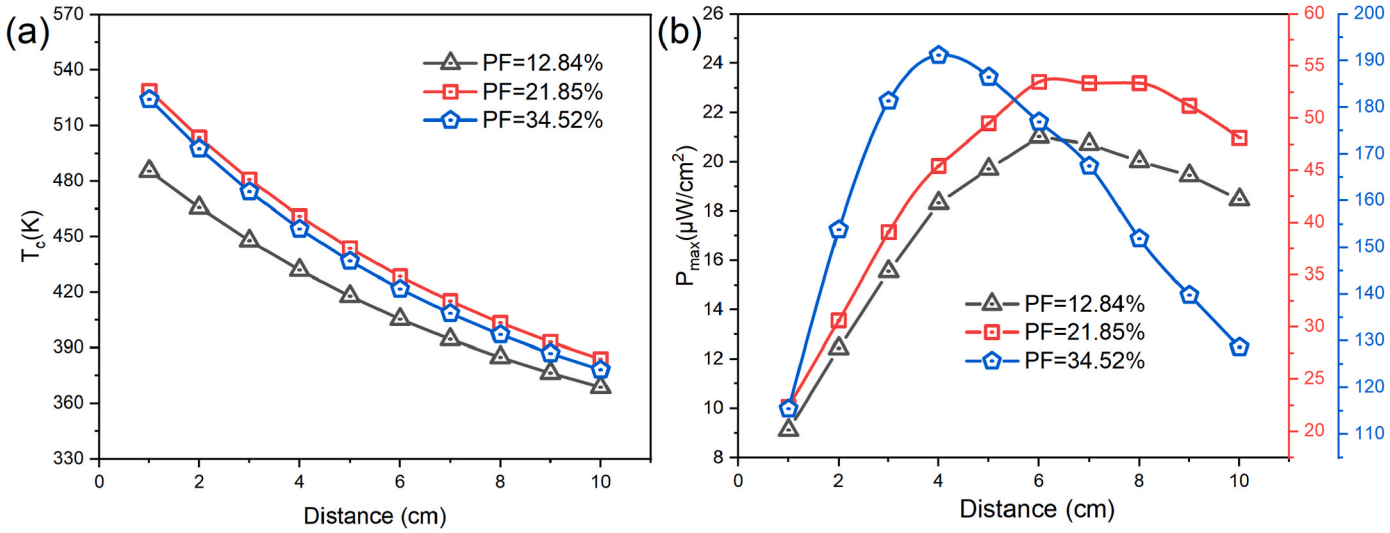

Fig. 8. Variation in (a) T_c and (b) P_{max} of InGaAs cell with the distance change under different heat source structures.

source shell can be considered as a kind of gray body coating, and its emissivity is 0.7–0.9, which also varies with temperature [31]. For the convenience of analysis, the emissivity of graphite was set as 0.8 on average in this study. The emissivity of the selective coating was often designed according to the cut-off wavelength of TPV cells. Here, the emissivity of the ideal and suboptimal coatings was set to 1.0 and 0.9 before 1800 nm, 0 and 0.1 after 1800 nm, respectively. The W@SiO_2 coating is a photonic crystal coating composed of metal tungsten (W) as the core and silicon dioxide (SiO_2) coated on the outside to form a core-shell ball, arranged in a certain way. The emissivity of the W@SiO_2 coating varies continuously with wavelength, so it was set as a continuous function [20]. All coatings described above could be changed by setting the boundary conditions of the emissivity, and the thickness were assumed to be small.

The thermal radiation power spectra of the radioisotope heat source with different coatings are shown in Fig. 2(b). The maximum surface temperatures (T_{max}) of the heat source covered by the graphite, ideal coating, suboptimal coating, and W@SiO_2 coating were 665 K, 1159 K, 1020 K, and 1011 K, respectively. The surface temperature of the heat source covered by the other three selective coatings was 346–504 K, which were higher than that of graphite. This phenomenon was due to the fact that the emissivity of the selective coating dropped sharply after the 1800 nm band, so part of infrared radiation could not be emitted effectively. In addition, the system thermal power was fixed, and the total thermal radiation was constant. To achieve the same amount of thermal radiation, the temperature of the heat source was continuously increased until the system reached thermal equilibrium. Increasing the temperature of the heat source also increased the available thermal radiation power. In the convertible band of TPV cell, the thermal radiation power of the selective coating was stronger than that of graphite, and the cell could receive more convertible energy and produce higher output performance. Therefore, suitable selective coatings can ensure that the radioisotope heat sources to generate higher temperature and more convertible thermal radiation power under specific thermal power conditions.

The electrical output performance of TPV cells is negatively correlated with the temperature they are exposed to (Fig. S4). In practical applications, TPV cells are usually kept at a certain distance from radioisotope heat source, which can reduce the negative effects of high temperature to a certain extent (experimental test results are shown in

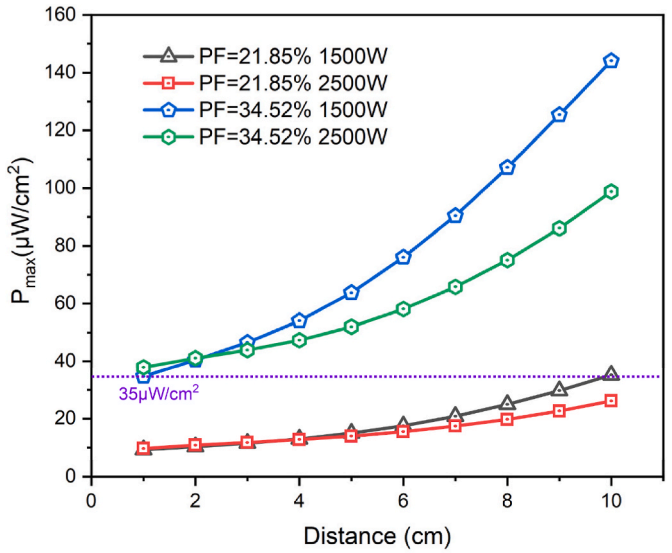

Fig. 9. Influence of thermal power on P_{max} with different heat source structures.

Figs. S5 and S6). To evaluate this effect, the distance between the InGaAs cell and the heat source was designed to vary from 1 cm to 10 cm. As shown in Fig. 3(a), the temperature (T_c) of the InGaAs cell decreased with increasing distance. The ideal coating, suboptimal coating and W@SiO_2 coating resulted in almost the same T_c, and the average T_c was only 6 K higher than that of the graphite coating in the range of 1–10 cm. Fig. 3(b) shows the maximum output power (P_{max}) of the InGaAs cell at different distances. The cell could attain a peak value of P_{max} within the designed coatings and distance range. As the distance increases, the temperature effect of the InGaAs cell weakens, and the intensity of infrared light received by the cell decreases. Combining these two opposite influences, the peak value of P_{max} could appear at a suitable position. The peak value of P_{max} with the graphite coating was at 6 cm, and the other three selective coatings were at 2 cm, while the corresponding T_{max} values were 665 K and above 1000 K. For approximately the same T_c, the available thermal radiation intensity of the radioisotope heat source was higher due to the influence of the selective coating.

By arranging the InGaAs cells parallel to the surface of the heat source, the volume of the RTPV was reduced by approximately 60 % by taking advantage of the selective coatings. The ideal coating led to the highest temperature and available spectral intensity, with a P_{max} of 107 mW/cm^2, which was considerably higher than those of the other cases (such as the P_{max} of 22 mW/cm^2 for the W@SiO_2 coating). Therefore, for the fixed power of the heat source, the selective coating not only caused the TPV cell temperature to rise less, but also enabled the TPV cell to generate higher electrical output at a position closer to the heat source. These effects are very beneficial for improving efficiency and miniaturizing RTPV.

3.2. Multi-module combination effect of heat source

To study the influence of multi-module combination of radioisotope heat sources on the RTPV performance, heat sources were vertically stacked. The number of heat sources vertically stacked was set from 1 to 10, so the thermal power of the heat source was varied from 250 W to 2500 W. Meanwhile, to avoid excessive variables caused by changing the coating, the emission characteristic of the heat source shell was still used for evaluation, graphite with an emissivity of 0.8 was considered as the coating.

As shown in Fig. 4, the multi-module combination of heat sources resulted in some beneficial changes to the maximum surface temperature (T_{max}). As the thermal power was increased, T_{max} increased, but the temperature rise tended to saturate. When the thermal power reached 1500 W, T_{max} was 705 K, but as the thermal power was increased to 2500 W, T_{max} was only 709 K. Thus, it could be concluded that there is no significant increase in T_{max} after the thermal power reached 1500 W. Through the multi-module combination of heat sources, that is, under constant thermal power density, T_{max} could be improved to a certain extent. According to the current results, the improvement effect of T_{max} was not remarkable, but it could still reach about 40 K within this evaluation range.

Fig. 5(a) shows the influence of the multi-module combination of heat sources on the temperature of InGaAs cells at different distances based on the finite element method. Compared with the case of 500 W heat source, T_c rose widely more than 50 K at each distance after increasing the thermal power. And T_c did not eventually tend to be same over the distance range evaluated. As shown in Fig. 5(b), the P_{max} of the InGaAs cell at 500 W was higher than that at other powers for the distances of 1–8 cm. When the thermal power was above 1000 W, the P_{max} increased monotonously in the range of 1–10 cm, with a maximum value of 22 μW/cm^2 at 10 cm. This is mainly because the combination of multi-module heat sources makes the temperature of the InGaAs cell rise obviously, but the generated infrared light by the heat sources improves slightly, and the influence of attenuation with distance is relatively weak. Furthermore, the peak value of P_{max} could be predicted to be higher and at a further distance when the thermal power exceeds 1000 W. This is due to the increase of the total radiant energy as the thermal power of heat source increases. Overall, using a multi-module combinatorial design for optimizing radioisotope heat sources resulted in a limited increase in the electrical output and a larger RTPV volume.

3.3. Packing factor for heat sources

The structure of the radioisotope heat source is also adjustable, and it

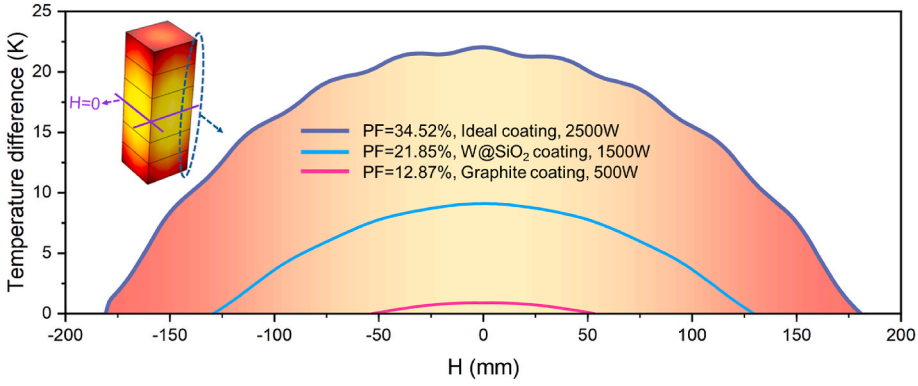

Fig. 10. Surface temperature distribution of isotopic heat sources.

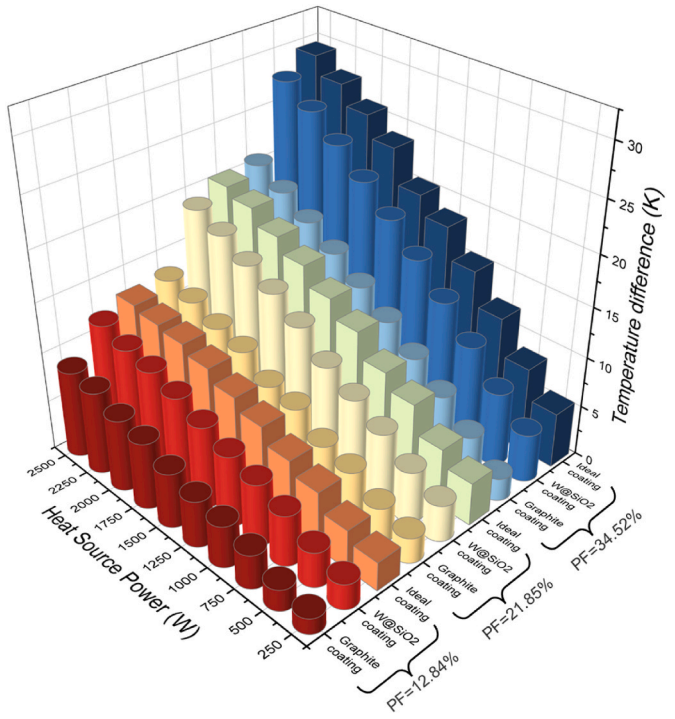

Fig. 11. The maximum temperature difference on the surface of isotopic heat source.

is possible to maintain better structural strength at smaller sizes [32,33]. To quantitatively describe the structural change of the heat source, the packing factor (*PF*) was defined here as the volume ratio of $^{238}PuO_2$ pellet to the overall heat source (V_{PuO2}/V_{Total}), which represents the thickness of the graphite shell covering the $^{238}PuO_2$ pellet. The $^{238}PuO_2$ pellet is set to be fixed and invariant, and the value of *PF* is increased by reducing the outer shell. The value of *PF* is 12.84 % in the initial case. However, the *PF* should not be too high, so that the graphite shell cannot completely cover the $^{238}PuO_2$ pellets, thereby destroying the structural integrity and stability. Based on this, further compact the structure and set the values of *PF* to 21.85 % (optimize case 1) and 34.52 % (optimize case 2), respectively, as shown in Fig. 6. The maximum surface temperature of isotopic heat source increased with increasing *PF* and changed approximately linearly in all three *PF* groups. After the *PF* was varied from 12.84 % to 34.52 %, the T_{max} increased by 115 K, when thermal power was 500 W and the surface emissivity was 0.8. Therefore, although *PF* was larger and the T_{max} was higher, the gain did not increase continuously because of the structural integrity of the heat source.

Even if the structure of the heat source changed, the thermal power still affected T_{max}. As shown in Fig. 7(a), the trend of T_{max} with several heat source structures had the same trend after the thermal power was increased. In addition, the improvement of T_{max} was not obvious after 1500 W. As shown in Fig. 7(b), the maximum T_{max} produced by increasing the thermal power may not reach the lower gain limit of changing the structure, so the influence of increasing thermal power on T_{max} was less than that of optimizing the heat source structure. Moreover, changes in the thermal power and structure of the heat source could also affect the neutron radiation characteristics, resulting in an increase in the neutron dose of the heat source. The calculation process and results of the neutron dose are shown in Figs. S7 and S8.

Fig. 8(a) shows the effect of the heat source structure on T_c at different distances. The increase in *PF* also made T_c rise at various distances, but the maximum temperature rise did not exceed 40 K, and the average temperature rise was approximately 23 K. The P_{max} values of the InGaAs cell with three structural heat sources are shown in Fig. 8(b). Compared with the case of *PF* = 12.84 %, the case of *PF* = 21.85 % generated a higher P_{max} and a flatter peak, which can be considered that a higher P_{max} could be obtained in the range of 6–8 cm. The case of *PF* = 34.52 % produced a P_{max} of 190 μW/cm^2, which was an order of magnitude higher than the case of *PF* = 12.84 %, primarily due to the increase in T_{max} and the enhancement of thermal radiation power spectrum. The peak value of P_{max} was at 4 cm, which was closer to the heat source than the other two cases, and the volume of RTPV could be reduced by 50 %. Thus, the optimized heat source structure could increase the electrical output density of RTPV by 10 times and make RTPV more compact.

Fig. 9 shows the variation in the electrical output of the InGaAs cell with distance when the thermal power of heat source was increased under different structures. As the distance increased, the P_{max} of the InGaAs cell increased monotonously with no peaks, and the excessive thermal power also led to a lower P_{max}. The P_{max} caused by the case of *PF* = 34.52 % was generally higher than that of *PF* = 21.85 %, which was mainly due to the higher temperature of the heat source at larger *PF*. When the thermal power was 1500 W, the maximum value of P_{max} generated by the case of *PF* = 21.85 % was 35 μW/cm^2, which was the same as the minimum value when *PF* = 34.52 %. Therefore, the gain of optimizing the heat source structure should be higher than that of increasing the thermal power in order to improve the P_{max} of RTPV.

3.4. Heat source surface temperature distribution

In the temperature regulation of isotopic heat source, balancing various factors is important for better temperature uniformity. To reduce the temperature gradients and make the thermal radiation power spectrum substantially consistent, a uniform surface temperature distribution is necessary for isotopic heat sources. The surface temperature difference (T_{max} - T_{min}) was used to evaluate the uniformity. Fig. 10 shows the temperature distribution at the vertical edge of isotopic heat sources. The abscissa represents the position of each point of the vertical edge, and the symmetrical center point of the vertical edge is at *H* = 0. Within the original design (graphite coating, thermal power of 500 W, and *PF* = 12.87 %), the temperature difference of the heat source was minimal or even negligible. When the heat source had an ideal coating, the thermal power was 2500 W, and *PF* was 34.52 %, the surface temperature difference can even go up to 22 K.

As shown in Fig. 11, it can be seen that with the increase of the thermal power and *PF*, the surface temperature difference increases gradually. And this tendency seems to be linear and does not tend to a stable value. The influence of the selective coating on the surface temperature difference is significantly greater than the gray body coating. Furthermore, compared with the ideal selective coating, the W@SiO_2 coating causes a smaller surface temperature difference. Therefore, selective coating, thermal power, and structural changes all lead to an increase in surface temperature difference, and the ideal effect can be achieved through comprehensive trade-offs.

4. Conclusion

A method for regulating and optimizing isotopic heat source temperature and corresponding electrical properties of RTPVs was proposed. The heat source temperature and available spectral intensity could be significantly improved by just using the optimized method of selective coating. The surface temperature of the heat source with the W@SiO_2 selective coating was 1011 K, the RTPV could produce a P_{max} of 22 mW/cm^2, and the volume can be reduced by 60 % compared to the initial situation. The use of selective coatings could maximize the temperature of isotopic heat source, allowing the TPV cells to produce higher electrical output and make RTPVs more compact. The research results contribute to understanding the temperature regulation mechanism of isotopic heat sources and improving the performance of RTPVs. This study can provide a certain reference solutions for more novel types

of RTPV designs and their future practical applications.

CRediT authorship contribution statement

Zhiheng Xu: Writing – original draft, Visualization, Project administration, Methodology, Funding acquisition, Formal analysis, Data curation, Conceptualization. **Jiyu Wang:** Writing – original draft, Methodology, Investigation, Formal analysis, Data curation. **Yuqiao Wang:** Supervision, Methodology, Conceptualization. **Shifan Zhu:** Validation, Methodology. **Hongyu Wang:** Validation, Software, Methodology. **Dandan Yang:** Writing – review & editing, Methodology, Conceptualization. **Yunpeng Liu:** Funding acquisition, Conceptualization. **Xiaobin Tang:** Writing – review & editing, Supervision, Resources, Methodology.

Declaration of competing interest

The authors declare that they have no known competing financial interests or personal relationships that could have appeared to influence the work reported in this paper.

Data availability

Data will be made available on request.

Acknowledgments

The authors would like to thank the scientific support kindly offered by the National Natural Science Foundation of China (Grant Nos. 12275132 and 12075119), and the Fundamental Research Funds for the Central Universities (Grant No. NT2023013).

Appendix A. Supplementary data

Supplementary data to this article can be found online at https://doi.org/10.1016/j.ijthermalsci.2024.109443.

References

[1] A. Mazzetti, M. Gianotti Pret, G. Pinarello, L. Celotti, M. Piskacev, A. Cowley, Heat to electricity conversion systems for moon exploration scenarios: a review of space and ground technologies, Acta Astronaut. 156 (2019) 162–186, https://doi.org/10.1016/j.actaastro.2018.09.025.

[2] M. Simon, K. Latorella, J. Martin, J. Cerro, R. Lepsch, S. Jefferies, et al., NASA's advanced exploration systems Mars transit habitat refinement point of departure design, IEEE Aerosp Conf Proc (2017), https://doi.org/10.1109/AERO.2017.7943662.

[3] T. Burger, C. Sempere, B. Roy-Layinde, A. Lenert, Present efficiencies and future opportunities in thermophotovoltaics, Joule 4 (2020) 1660–1680, https://doi.org/10.1016/j.joule.2020.06.021.

[4] A. Datas, A. Martí, Thermophotovoltaic energy in space applications: review and future potential, Sol. Energy Mater. Sol. Cells 161 (2017) 285–296, https://doi.org/10.1016/j.solmat.2016.12.007.

[5] M.A. Prelas, C.L. Weaver, M.L. Watermann, E.D. Lukosi, R.J. Schott, D. A. Wisniewski, A review of nuclear batteries, Prog. Nucl. Energy 75 (2014) 117–148, https://doi.org/10.1016/j.pnucene.2014.04.007.

[6] R.G. Lange, W.P. Carroll, Review of recent advances of radioisotope power systems, Energy Convers. Manag. 49 (2008) 393–401, https://doi.org/10.1016/j.enconman.2007.10.028.

[7] T.J. Coutts, Review of progress in thermophotovoltaic generation of electricity, Renew. Sustain. Energy Rev. 3 (1999) 77–184, https://doi.org/10.1016/S1364-0321(98)00021-5.

[8] A. Schock, M. Mukunda, C. Or, V. Kumar, G. Summers, Design, analysis, and optimization of a radioisotope thermophotovoltaic (RTPV) generator, and its applicability to an illustrative space mission, Acta Astronaut. 37 (1995) 21–57, https://doi.org/10.1016/0094-5765(95)00071-7.

[9] R.D. Lorenz, E.S. Clarke, Influence of the multi-Mission radioisotope thermoelectric generator (MMRTG) on the local atmospheric environment, Planet. Space Sci. 193 (2020) 105075, https://doi.org/10.1016/j.pss.2020.105075.

[10] R.M. Ambrosi, H. Williams, E.J. Watkinson, A. Barco, R. Mesalam, T. Crawford, et al., European radioisotope thermoelectric generators (RTGs) and radioisotope heater units (RHUs) for space science and exploration, Space Sci. Rev. 215 (2019) 55, https://doi.org/10.1007/s11214-019-0623-9.

[11] C. Ferrari, F. Melino, M. Pinelli, P.R. Spina, Thermophotovoltaic energy conversion: analytical aspects, prototypes and experiences, Appl. Energy 113 (2014) 1717–1730, https://doi.org/10.1016/j.apenergy.2013.08.064.

[12] A. Schock, C. Or, V. Kumar, Small radioisotope thermophotovoltaic (RTPV) generators, AIP Conf. Proc. 358 (1996) 81–97, https://doi.org/10.1063/1.49711.

[13] M.D. Morgan, W.E. Horne, P.R. Brothers, Radioisotope thermophotovoltaic power system utilizing the GaSb IR photovoltaic cell, AIP Publishing 313 (2008) 271, https://doi.org/10.1063/1.43167.

[14] S.J. Cheon, S.G. Hong, J.H. Lee, Y.S. Nam, Design and performance analysis of a 500-W heat source for radioisotope thermophotovoltaic converters, Int. J. Energy Res. 42 (2018) 817–829, https://doi.org/10.1002/er.3889.

[15] X. Wang, R. Liang, P. Fisher, W. Chan, J. Xu, Radioisotope thermophotovoltaic generator design methods and performance estimates for space missions, J Propuls Power 36 (2020) 593–603, https://doi.org/10.2514/1.B37623.

[16] X. Wang, W.R. Chan, V. Stelmakh, M. Soljacic, J.D. Joannopoulos, I. Celanovic, et al., Prototype of radioisotope thermophotovoltaic system using photonic crystal spectral control, J Phys Conf Ser 660 (2015) 012034, https://doi.org/10.1088/1742-6596/660/1/012034.

[17] J. Lee, S. Cheon, S. Hong, Y. Nam, A radioisotope thermophotovoltaic converter with nanophotonic emitters and filters, Int J Heat Mass Transf 108 (2017) 1115–1125, https://doi.org/10.1016/j.ijheatmasstransfer.2016.12.049.

[18] H. Wang, X. Tang, Y. Liu, Z. Xu, Z. Yuan, K. Liu, et al., Thermal emission-enhanced and optically modulated radioisotope thermophotovoltaic generators, Energy Technol. 8 (2020) 1901170, https://doi.org/10.1002/ente.201901170.

[19] H. Wang, Z. Xu, Z. Yuan, K. Liu, C. Meng, X. Tang, High-temperature and radiation-resistant spinel-type ferrite coating for thermo-optical conversion in radioisotope thermophotovoltaic generators, Energy 239 (2022) 122255, https://doi.org/10.1016/j.energy.2021.122255.

[20] C. Meng, Y. Liu, Z. Xu, H. Wang, X. Tang, Selective emitter with core–shell nanosphere structure for thermophotovoltaic systems, Energy 239 (2022) 121884, https://doi.org/10.1016/j.energy.2021.121884.

[21] A. Molki, Temperature effect on photovoltaic cells, Phys. Educ. 11 (2011) 62–73, https://doi.org/10.1088/0031-9120/46/5/F08.

[22] C. Zhang, Z. Liao, L. Tang, Z. Liu, R. Huo, Z. Wang, et al., A comparatively experimental study on the temperature-dependent performance of thermophotovoltaic cells, Appl. Phys. Lett. 114 (2019) 193902, https://doi.org/10.1063/1.5088791.

[23] X. Peng, B. Zhang, G. Li, J. Zou, Z. Zhu, Z. Cai, et al., Simulation of temperature-dependent material parameters and device performances for GaInAsSb thermophotovoltaic cell, Infrared Phys. Technol. 54 (2011) 454–459, https://doi.org/10.1016/j.infrared.2011.08.005.

[24] E. Blandre, R. Vaillon, J. Drévillon, New insights into the thermal behavior and management of thermophotovoltaic systems, Opt Express 27 (2019) 36340, https://doi.org/10.1364/oe.27.036340.

[25] G.L. Bennett, J.J. Lombardo, R.J. Hemler, G. Silverman, C.W. Whitmore, W. R. Amos, et al., Mission of daring: the general-purpose heat source radioisotope thermoelectric generator, Collect Tech Pap - 4th Int Energy Convers Eng Conf 1 (2006) 720–742, https://doi.org/10.2514/6.2006-4096.

[26] R.C. O'Brien, R.M. Ambrosi, N.P. Bannister, S.D. Howe, H.V. Atkinson, Safe radioisotope thermoelectric generators and heat sources for space applications, J. Nucl. Mater. 377 (2008) 506–521, https://doi.org/10.1016/j.jnucmat.2008.04.009.

[27] S. Shittu, G. Li, X. Zhao, Y.G. Akhlaghi, X. Ma, M. Yu, Comparative study of a concentrated photovoltaic-thermoelectric system with and without flat plate heat pipe, Energy Convers. Manag. 193 (2019) 1–14, https://doi.org/10.1016/j.enconman.2019.04.055.

[28] W. Tao, Heat Transfer, fifth ed., Higher Education Press, Beijing, 2019, pp. 337–375 (In Chinese).

[29] J.R. Howell, M.P. Mengüç, K. Daun, et al., Thermal Radiation Heat Transfer, CRC Press, 2020, pp. 113–155, https://doi.org/10.1201/9780429327308.

[30] B. Roy-Layinde, T. Burger, D. Fan, B. Lee, S. McSherry, S.R. Forrest, et al., Sustaining efficiency at elevated power densities in InGaAs airbridge thermophotovoltaic cells, Sol. Energy Mater. Sol. Cells 236 (2022) 111523, https://doi.org/10.1016/j.solmat.2021.111523.

[31] G. Neuer, Emissivity measurements on graphite and composite materials in the visible and infrared spectral range, Quant. InfraRed Thermogr. 92 (1992), https://doi.org/10.21611/qirt.1992.056.

[32] J.G. Teague, R.N. Mulford, Impact temperature determination for GPHS safety testing, Nucl. Technol. 206 (2020) 1195–1212, https://doi.org/10.1080/00295450.2019.1701345.

[33] S. Shiri, A robust optimization approach for design of a General Purpose Heat Source, J Sp Saf Eng 8 (2021) 211–216, https://doi.org/10.1016/j.jsse.2021.07.006.